

Allocating and splitting free energy to maximize molecular machine flux

Aidan I. Brown* and David A. Sivak*

Department of Physics, Simon Fraser University, Burnaby, BC, V5A1S6 Canada

E-mail: aidanb@sfu.ca; dsivak@sfu.ca

Abstract

Biomolecular machines transduce between different forms of energy. These machines make directed progress and increase their speed by consuming free energy, typically in the form of nonequilibrium chemical concentrations. Machine dynamics are often modeled by transitions between a set of discrete metastable conformational states. In general, the free energy change associated with each transition can increase the forward rate constant, decrease the reverse rate constant, or both. In contrast to previous optimizations, we find that in general flux is neither maximized by devoting all free energy changes to increasing forward rate constants nor by solely decreasing reverse rate constants. Instead the optimal free energy splitting depends on the detailed dynamics. Extending our analysis to machines with vulnerable states (from which they can break down), in the strong driving corresponding to *in vivo* cellular conditions, processivity is maximized by reducing the occupation of the vulnerable state.

Introduction

Molecular machines such as kinesin,¹ helicase,² and ubiquitin ligase³ perform diverse tasks inside cells. These machines typically convert nonequilibrium chemical concentrations, maintained by other machinery in the cell,^{4,5} into directed motion or work.^{6,7} These microscopic machines operate stochastically,⁸ with their fluctuating progress now experimentally observable with improving resolution (see *e.g.* Isojima *et al*⁹).

Quantitative models of molecular machines are pervasive, *e.g.* to investigate forces,¹⁰ efficiency,¹¹ and performance of different driving mechanisms.^{12,13} Each model usually treats molecular machine dynamics as a set of transitions between discrete metastable states,¹⁴ as diffusion on a continuous energy landscape,¹⁵ or a combination of the two.¹⁶

In this paper we study how the flux of cyclic machines, a posited driver of evolutionary fitness,¹⁷ is affected by the details of free energy changes over a set of discrete states.

Earlier models considered how the influence of a load is quantitatively split between forward and reverse transitions.^{10–12,14} In this work we find that by extending the splitting to all free energy components, not just loads, there is no single splitting scheme that always maximizes the flux. Additionally, optimizing the allocation of a single free energy component compensates for any sub-optimal fixed allocations of other free energy components.

We also examine how to maximize progress for transiently processive cyclic machines with vulnerable states, from which the machine can break down or ‘escape’ (*e.g.* kinesin can dissociate from a microtubule¹⁸). For strong driving, free energy is simply allocated to reduce the occupation of the state vulnerable to escape. However, under specific conditions, the optimal allocation is reversed, counterintuitively increasing processivity by increasing occupation of the vulnerable state.

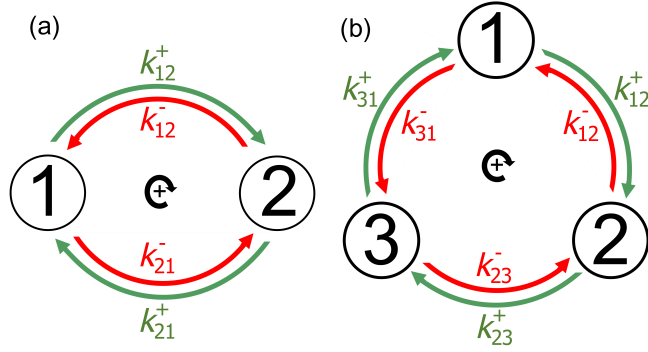


Figure 1: **Discrete-state cycles with (a) two and (b) three states.** Transitions occur in both the forward (green arrows) and reverse (red arrows) directions for each pathway between two states, described by respective rate constants k_{ij}^+ and k_{ij}^- .

Model

Discrete states

We consider cycles with two or three states (Fig. 1), often used for models of molecular motors or other driven systems inside living cells.^{19,20} For our model cycles, each forward rate constant k_{ij}^+ describes transitions from state i to state j , with a corresponding reverse rate constant k_{ij}^- for transitions from state j to state i . To preserve microscopic reversibility,^{10,13} any transition with a nonzero forward rate cannot be irreversible, and must also have a nonzero reverse rate.

Forward transitions from state i to state j occur at rate $k_{ij}^+ P_i$, for probability P_i in state i . Reverse transitions from state j to state i occur at reverse rate $k_{ij}^- P_j$. (The two-state cycle has two pathways, 12 and 21, each with a forward and reverse direction, and each representing distinguishable physical transition mechanisms.)

To preferentially drive such cycles in a particular direction, cells use nonequilibrium concentrations of reacting chemical species, such as adenosine triphosphate (ATP), adenosine diphosphate (ADP), and inorganic phosphate (P_i).²¹ ATP hydrolysis into ADP and P_i yields a free energy ΔG that depends on the respective concentrations,²¹

$$\Delta G = \Delta G_0 + k_B T \ln \frac{[\text{ADP}][P_i]}{[\text{ATP}]} . \quad (1)$$

Here $\Delta G_0 \equiv -k_B T \ln ([\text{ADP}]_{\text{eq}}[P_i]_{\text{eq}}/[\text{ATP}]_{\text{eq}})$, k_B is Boltzmann's constant, and T is the temperature of the thermal bath exchanging heat with the system. ATP hydrolysis provides free energy $|\Delta G| \sim 20k_B T$ under typical physiological conditions.²¹ From here on we set $k_B T = 1$, thus measuring all free energies in units of the thermal energy scale $k_B T$.

The free energy allocation ω_{ij} of a given transition path fixes the ratio between the forward and reverse rate constants,^{12,22,23}

$$\omega_{ij} = \ln \frac{k_{ij}^+}{k_{ij}^-} . \quad (2)$$

Without ω_{ij} to provide a bias, the full forward and reverse rate constants $k_{ij}^{+/-}$ each equal the 'bare' rate constants k_{ij}^0 . $\omega_{ij} = -\Delta G_{ij}$, where ΔG_{ij} is the free energy change of the machine and its surroundings over the transition. ΔG over a given cycle must be negative to drive net progress in the forward direction (on average).

Biasing rates with free energy

ω_{ij} can be composed of several different free energy components, including but not limited to conformational changes, binding/unbinding, or a change in potential.

The free energy change $\Delta G_{ij}^{\text{mach}}$ of the molecular machine over a transition includes free energy differences between distinct machine conformations, as well as changes in the free energy of any molecules bound to the machine (*e.g.* hydrolysis of ATP to ADP and P_i), as the free energy changes of the machine and bound species cannot be separated.^{24,25}

$\Delta G_{ij}^{\text{bind}} = -\mu$ is the free energy change of the solution when a molecule binds the machine, leaving the solution, with μ the chemical potential of the molecule given the concentration in solution. $\Delta G_{ij}^{\text{bind}}$ includes molecules typically considered ‘fuel’, such as ATP; and those typically considered cargo. For a molecule that unbinds from the machine and joins the solution, $\Delta G_{ij}^{\text{unbind}} = \mu$.

$\Delta G_{ij}^{\text{pot}}$ represents the free energy change of the machine, or any object attached to the machine, due to an external potential or gradient, *e.g.* due to a bead attached to kinesin that is also in an optical trap.

We confine our attention in this paper to ‘reversible’ free energy components, whereby any free energy expended in a forward reaction is recovered by the reverse reaction. Thus we exclude from consideration any omnidirectional free energy dissipation, such as that due to friction when pulling a load through a viscous medium.

Excepting $\Delta G_{ij}^{\text{mach}}$, we expect that the free energy components are relatively fixed (*i.e.* unable to be changed by a modification to the machine). $\sum \Delta G_{ij}^{\text{mach}} = 0$, as the machine returns to the same state after completing each cycle – abiding by this constraint, variation of $\Delta G_{ij}^{\text{mach}}$ (nominally through machine mutations) can be used to optimize machine operation.

We model each free energy component $\omega_{ij}^k = -\Delta G_{ij}^k$ with a different splitting factor^{11,12} $\delta_{ij}^k \in [0, 1]$, which describes how the effect of ω_{ij}^k is divided between forward and reverse rate constants,

$$k_{ij}^+ \propto e^{\sum_k \delta_{ij}^k \omega_{ij}^k} \quad \text{and} \quad k_{ij}^- \propto e^{-\sum_k (1-\delta_{ij}^k) \omega_{ij}^k} . \quad (3)$$

Earlier studies^{10–12,14} considered a molecular motor pulling against a constant opposing force F , with each cycle of the motor stepping forward a distance d . The transition completing the step transduces free energy $w = Fd$ to the motor’s position in the potential. In our framework this corresponds to $\omega_{ij}^{\text{pot}} = -w$. For steps against this constant force, $\delta_{ij}^{\text{pot}} = 0$ is known as a *power stroke* (PS) and $\delta_{ij}^{\text{pot}} = 1$ is known as a *Brownian ratchet* (BR).¹²

In this paper we primarily consider the case where splitting factors δ_{ij}^k have the same value δ for all free energy components. This simple framework assumes the transition state is similarly arrayed between the reactant and product along different coordinate axes. We label $\delta = 1$ as *forward labile* (FL) and $\delta = 0$ as *reverse labile* (RL). FL is then similar to BR, and RL to PS.²⁶ The choice between PS and BR, or between FL and RL, affects machine performance characteristics,^{12,26} and below we determine how to vary splitting factors to maximize flux.

Maximizing flux

Optimal splitting factors

Setting all splitting factors δ_{ij}^k to the same value δ allows the combination of all $\delta_{ij}^k \omega_{ij}^k$ terms in Eqs. 3 into single terms $\delta \omega_{ij}$ and $(1 - \delta) \omega_{ij}$, giving rate constants

$$k_{ij}^+ = k_{ij}^0 e^{\delta \omega_{ij}} , \quad (4a)$$

$$k_{ij}^- = k_{ij}^0 e^{-(1-\delta) \omega_{ij}} . \quad (4b)$$

We consider a two-state cycle, with steady-state flux (hereafter simply flux)²⁷

$$J = \frac{k_{12}^+ k_{21}^+ - k_{12}^- k_{21}^-}{k_{12}^+ + k_{12}^- + k_{21}^+ + k_{21}^-} . \quad (5)$$

Inserting Eq. 4 into Eq. 5 and differentiating with respect to δ gives

$$\frac{\partial J}{\partial \delta} = \frac{(1 - e^{-\omega_{\text{tot}}}) \left[\frac{k_{12}^0 \omega_{21} e^{-\delta \omega_{21}} (1 + e^{-\omega_{12}}) + k_{21}^0 \omega_{12} e^{-\delta \omega_{12}} (1 + e^{-\omega_{21}})}{(k_{21}^0)^{-1} e^{-\delta \omega_{21}} (1 + e^{-\omega_{12}}) + (k_{12}^0)^{-1} e^{-\delta \omega_{12}} (1 + e^{-\omega_{21}})} \right]}{\left[\frac{k_{12}^0 \omega_{21} e^{-\delta \omega_{21}} (1 + e^{-\omega_{12}}) + k_{21}^0 \omega_{12} e^{-\delta \omega_{12}} (1 + e^{-\omega_{21}})}{(k_{21}^0)^{-1} e^{-\delta \omega_{21}} (1 + e^{-\omega_{12}}) + (k_{12}^0)^{-1} e^{-\delta \omega_{12}} (1 + e^{-\omega_{21}})} \right]^2} . \quad (6)$$

The cycle proceeds forward when $\omega_{\text{tot}} = \omega_{12} + \omega_{21} > 0$. $\partial J / \partial \delta > 0$ for all δ when both $\omega_{12} > 0$ and $\omega_{21} > 0$; for these conditions, $\delta = 1$ (FL) maximizes the flux. For $\delta = 0$ (RL) to maximize the flux requires

$$k_{12}^0 \omega_{21} (1 + e^{-\omega_{12}}) e^{-\delta \omega_{21}} + k_{21}^0 \omega_{12} (1 + e^{-\omega_{21}}) e^{-\delta \omega_{12}} < 0 , \quad (7)$$

a more complicated condition to fulfill, as $\omega_{12} < 0$ and $\omega_{21} < 0$ cannot be simultaneously fulfilled with $\omega_{\text{tot}} > 0$. Flux can also be maximized for intermediate δ , with $\partial J / \partial \delta$ changing sign (maximizing flux) when

$$\delta = \frac{1}{\omega_{21} - \omega_{12}} \ln \left[- \frac{k_{12}^0 \omega_{21} (1 + e^{-\omega_{12}})}{k_{21}^0 \omega_{12} (1 + e^{-\omega_{21}})} \right] . \quad (8)$$

The flux-maximizing value of splitting factor δ thus depends on free energy allocation ω_{ij} and bare rate constants k_{ij}^0 .

Although here we set $\delta_{ij}^k = \delta$, in Supplemental Information (SI): Varying splitting factors, we consider splitting factors δ_{ij}^k that vary across different free energy components and different transitions. Notably, for splitting factors specific to each free energy component k and transition ij , if $\omega_{ij}^k < 0$ then $\delta_{ij}^k = 0$ maximizes the flux, and if $\omega_{ij}^k > 0$ then $\delta_{ij}^k = 1$ maximizes the flux.

For a molecular motor pulling against a constant force, a forward step has free energy component $\omega_{ij}^{\text{pot}} = -w < 0$. For independent variation of δ_{ij}^k , flux is maximized for $\delta_{ij}^{\text{pot}} = 0$. In this scenario, the optimal splitting factor agrees with Wagoner and Dill's finding that $\delta = 0$ maximizes the power.¹² Our results are generally distinct, and do not find a universal optimal δ value, because we generalize to cycles with multiple states and splitting factors that apply to all free energy components, not just the free energy component associated with pulling against a constant force.

Fig. 2 shows the variation in flux as the splitting factor δ is varied from the flux-maximizing value in the range $\delta \in [0, 1]$. The flux can be maximized at an extreme splitting factor value, $\delta = 1$ (left panels) or 0 (not shown, but possible), or between the extreme values, $\delta \in (0, 1)$ (right panels). The flux can decrease by more than an order of magnitude away from the optimal δ value, and decreases faster for larger ω_{tot} .

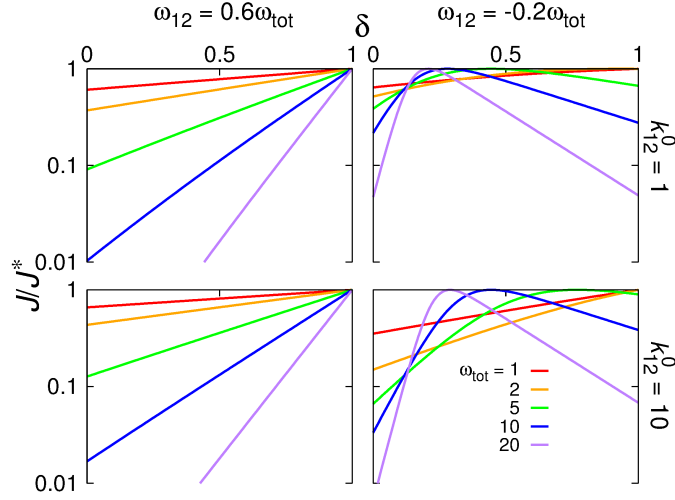


Figure 2: **Two-state flux sensitivity to splitting factor.** Flux ratio J/J^* as a function of the splitting factor δ , for a two-state cycle with bare rate $k_{21}^0 = 1$. k_{12}^0 , ω_{tot} , and ω_{12} vary as indicated. J is given by substituting the rate constants of Eq. 4 into Eq. 5. J^* is determined in the range $\delta \in [0, 1]$. Optimal flux J^* is specific to each curve on each subplot.

Optimal free energy allocation

Considering Eq. 4, we vary the free energy ω_{ij} allocated to each transition to adjust the rate constants and maximize the flux.

For the total free energy budget per cycle $\omega_{\text{tot}} = \omega_{12} + \omega_{21}$, the flux-maximizing free energy allocation ω_{12}^* satisfies (see SI: Varying free energy)

$$k_{12}^0 e^{\delta \omega_{12}^*} [\delta - (1 - \delta) e^{-\omega_{12}^*}] = k_{21}^0 e^{\delta(\omega_{\text{tot}} - \omega_{12}^*)} [\delta - (1 - \delta) e^{-(\omega_{\text{tot}} - \omega_{12}^*)}] . \quad (9)$$

This cannot generally be solved for ω_{12}^* .

For equal splitting factors $\delta_{ij}^k = \delta$, rate constants are determined by the sum of all free energy components $\sum_k \omega_{ij}^k$, such that if all but one free energy component is fixed, the remaining free energy component can be varied to achieve any desired sum. This makes maximal flux attainable by only adjusting the free energy allocation of the molecular machine, $\Delta G_{ij}^{\text{mach}}$.

For $\delta = 0$ and 1 the rate constants reduce to those of our previous work,²⁶ from which the flux-maximizing free energy allocation ω_{ij}^* can be determined. For $\delta = 1$ (FL),

$$\omega_{12}^* = \frac{1}{2} \omega_{\text{tot}} + \frac{1}{2} \ln \frac{k_{21}^0}{k_{12}^0} . \quad (10)$$

For $\delta = 0$ (RL),

$$\omega_{12}^* = \frac{1}{2} \omega_{\text{tot}} - \frac{1}{2} \ln \frac{k_{21}^0}{k_{12}^0} . \quad (11)$$

ω_{ij} may be decomposed into multiple free energy components; for conceptual clarity we limit our discussion to two, $\omega_{ij} = \omega_{ij}^{\text{I}} + \omega_{ij}^{\text{II}}$, but our results trivially generalize. With $\omega_{ij}^* = \omega_{ij}^{\text{I}*} + \omega_{ij}^{\text{II}*}$, $\sum \omega_{ij}^{\text{I}} = \omega_{\text{tot}}^{\text{I}}$, and $\sum \omega_{ij}^{\text{II}} = \omega_{\text{tot}}^{\text{II}}$, then for $\delta = 1$, Eq. 10 becomes

$$\omega_{12}^{\text{I}*} + \omega_{12}^{\text{II}*} = \frac{1}{2} (\omega_{\text{tot}}^{\text{I}} + \omega_{\text{tot}}^{\text{II}}) + \frac{1}{2} \ln \frac{k_{21}^0}{k_{12}^0} . \quad (12)$$

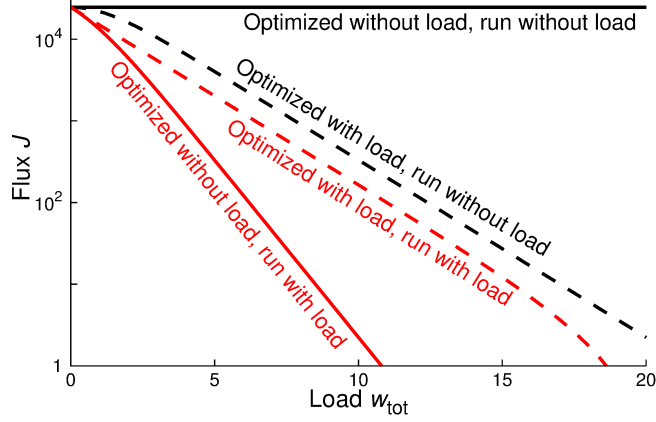


Figure 3: **Robustness to variable load.** Flux J vs. load w_{tot} for a two-state forward labile ($\delta_{ij}^k = \delta = 1$) cycle. The load is entirely on the first transition, $\omega_{12}^{\text{II}} = -w_{\text{tot}}$, and $\omega_{21}^{\text{II}} = 0$. Bare rate constants $k_{12}^0 = 5$, $k_{21}^0 = 1$, and load-free free energy budget $\omega_{\text{tot}}^{\text{I}} = 20$. Solid curves are for $\omega_{ij}^{\text{I}, \text{no load}}$ optimized for no load, while dashed curves are for $\omega_{ij}^{\text{I}, \text{load}}$ optimized with load w_{tot} . Black curves show flux without load ($w_{\text{tot}} = 0$), while red curves show flux with load w_{tot} as indicated by the horizontal axis.

If one component is fixed (without loss of generality ω_{ij}^{II}), then ω_{ij}^{I} can vary to preserve the flux-maximizing allocation $\omega_{ij}^* = \omega_{ij}^{\text{I},*} + \omega_{ij}^{\text{II},*}$. Effectively, the variable component of ω_{ij} can compensate for the fixed component to maximize the flux.

In earlier work,²⁶ we showed that for a range of several $k_{\text{B}}T$ around the optimal allocation, the flux can decrease by more than an order of magnitude. The free energy allocation can thus meaningfully alter the cycle output.

In this section we considered equal splitting factors for all free energy components and transitions: $\delta_{ij}^k = \delta$. In SI: Varying free energy, we consider the more general case where the splitting factor varies over free energy components and transitions, similarly finding that variable free energy components compensate for fixed components.

Robustness to variable load

The *in vivo* operating environment of molecular machines is diverse, with variable cargo, molecular concentrations, and other factors causing some free energy components to vary over the life-cycle of a machine. We consider a scenario with two free energy components over a cycle, $\omega_{\text{tot}}^{\text{I}}$ and $\omega_{\text{tot}}^{\text{II}}$. $\omega_{\text{tot}}^{\text{I}}$ has some fixed value, but $\omega_{\text{tot}}^{\text{II}}$ is a load that can be applied or removed, with $\omega_{\text{tot}}^{\text{II}} = 0$ (no load) or $\omega_{\text{tot}}^{\text{II}} = -w_{\text{tot}} < 0$ (load). The allocation of $\omega_{\text{tot}}^{\text{II}}$ to the various ω_{ij}^{II} is fixed. If the allocation of ω_{ij}^{I} is optimized without (with) an applied load, but then the load is applied (removed), the flux will generally be lower than if ω_{ij}^{I} is optimized under the correct conditions. Fig. 3 shows the flux as a function of load for $\omega_{\text{tot}}^{\text{I}} = 20k_{\text{B}}T$ (that of ATP at physiological conditions) for the four possible scenarios, optimized with ($\omega_{ij}^{\text{I}, \text{load}}$) or without load ($\omega_{ij}^{\text{I}, \text{no load}}$) and subsequently applying or not applying a load.

The fluxes for the four scenarios have a fixed order, independent of model parameters. Without load, cycle flux is higher under the correctly optimized allocation $\omega_{ij}^{\text{I}, \text{no load}}$ than under $\omega_{ij}^{\text{I}, \text{load}}$ incorrectly optimized for load; under $\omega_{ij}^{\text{I}, \text{load}}$ the flux is higher without load than with, because adding a resistive load always reduces the flux; and with load, flux under the correctly optimized $\omega_{ij}^{\text{I}, \text{load}}$ is higher than under the incorrectly optimized $\omega_{ij}^{\text{I}, \text{no load}}$. Due to this fixed ordering, the flux changes less when the load is applied or removed if the free energy component allocation is optimized with a load ($\omega_{ij}^{\text{I}, \text{load}}$), compared to if the allocation is optimized for no load ($\omega_{ij}^{\text{I}, \text{no load}}$).

Processivity

Many cycles are transiently processive, eventually ‘escaping’ from their processive mode of operation, precluding further progress. For example, a transport motor can detach from its cytoskeletal track and diffuse away, effectively ending its forward transport.^{18,28}

We model escape from a single ‘vulnerable’ state (without loss of generality, state 2), consistent with experiments suggesting kinesin primarily detaches from a subset of states.^{18,29–32} The vulnerable state has an escape rate constant k_{esc} . The states which are not vulnerable have the same dynamics as earlier. For the two-state cycle, escape produces modified state 2 dynamics

$$\frac{dP_2}{dt} = (k_{12}^+ + k_{21}^-)P_1 - (k_{12}^- + k_{21}^+)P_2 - k_{\text{esc}}P_2 . \quad (13)$$

For $k_{\text{esc}} > 0$, probability leaves the cycle and there are no steady states for occupation probabilities P_i (except $P_1 = P_2 = 0$). Instead, we find steady states for the fractional probabilities P_i/P_{tot} (see SI: Processivity), for total remaining probability $P_{\text{tot}} = \sum_i P_i$. This determines the dynamics of P_{tot} , and thus the average fluxes in the cycle at all times t : $P_{\text{tot}}(t) = \exp[-k_{\text{esc}}(P_2/P_{\text{tot}})t]$.

Unlike a cycle without escape, in the steady state of P_i/P_{tot} the fluxes for the different transitions will not generally be equal. For the two-state cycle, the changes in probabilities P_1, P_2 are determined by the flux into and out of the respective states:

$$\frac{dP_1}{dt} = J_{21} - J_{12} \quad (14a)$$

$$\frac{dP_2}{dt} = J_{12} - J_{21} - J_{\text{esc}} . \quad (14b)$$

Once P_i/P_{tot} reaches steady state, $dP_i/dt = P_i d \ln P_{\text{tot}}/dt$. Substituting this into Eqs. 14 and rearranging gives the pathway (or one-sided) steady-state flux

$$J_{12} = J_{21} + \frac{P_1}{P_1 + P_2} J_{\text{esc}} . \quad (15)$$

Accumulated flux

Because the flux decays with time as probability escapes, we additionally include the rate of escape in our evaluation of molecular machine progress. Instead of flux alone, we combine flux and (avoided) escape into the ‘accumulated flux’,

$$\Phi_{\text{acc}}(t) = \int_0^t [J_{12}(t') + J_{21}(t')] dt' . \quad (16)$$

For $t \rightarrow \infty$, Φ_{acc} can always be increased by adjusting ω_{ij} to reduce P_2/P_{tot} and thus reduce escape, so $\Phi_{\text{acc}}(\infty)$ has no maximum, hence we maximize $\Phi_{\text{acc}}(t)$ after a finite time t .

For simplicity, we consider two-state cycles with a single splitting factor $\delta_{ij}^k = \delta$. We set bare rate constants $k_{12}^0 = k_{21}^0 = 1$, such that all escape rate constants k_{esc} are in units of this bare rate. Fig. 4 shows two-state free energy allocations that maximize accumulated flux $\Phi_{\text{acc}}(t)$ for FL and RL schemes at various finite times t , for two distinct escape rate constants k_{esc} (see SI: Processivity for similar three-state results). These escape rate constants are consistent with modeling that suggests the detachment timescale from the vulnerable state of myosin V is 10-1000× slower than other timescales in the main forward pathway at zero force.³³

A prominent feature of Fig. 4 is the approximate collapse of cycles with different k_{esc} to the same

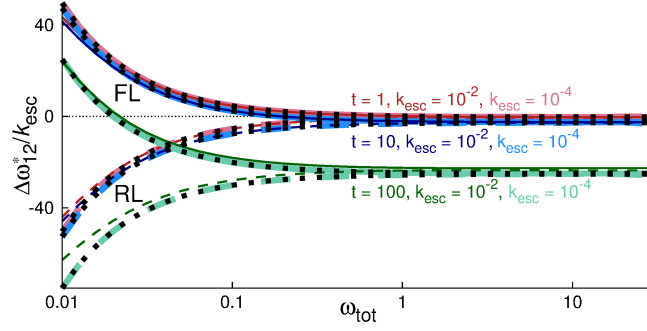


Figure 4: **Allocating free energy to maximize processivity.** Free energy allocation ω_{12} that maximizes accumulated flux Φ_{acc} (Eq. 16) over varying integration times t (indicated by curve color), in a FL (solid lines) or RL (dashed) two-state cycle with $k_{12}^0 = k_{21}^0 = 1$ and escape rate $k_{\text{esc}} = 10^{-2}$ or 10^{-4} . Thick black dotted curves show Eqs. 17 and 18, which approximate $\Delta\omega_{12}^*/k_{\text{esc}}$ with low k_{esc} for FL and RL, respectively. Allocation is shown as the difference $\Delta\omega_{ij}^* = \omega_{ij}^* - \frac{1}{2}\omega_{\text{tot}}$ from the ‘naive’ allocation of equal free energy $\frac{1}{2}\omega_{\text{tot}}$ to each transition. $\Delta\omega_{21}^* = -\Delta\omega_{12}^*$ is not shown. Initial condition is steady state for P_i/P_{tot} .

$\Delta\omega_{12}^*/k_{\text{esc}}$ (where $\Delta\omega_{12}^* = \omega_{12} - \frac{1}{2}\omega_{\text{tot}}$), demonstrating that the optimal free energy allocation $\Delta\omega_{12}^* \propto k_{\text{esc}}$ for the parameter values shown in Fig. 4 (SI: Processivity shows optimal allocations for larger t , which do not collapse). For FL cycles with small k_{esc} and t ,

$$\frac{\Delta\omega_{12}^*}{k_{\text{esc}}} \simeq -\frac{1}{4} \left(t - \frac{1}{e^{\frac{1}{2}\omega_{\text{tot}}} - 1} \right), \quad (17)$$

and for RL,

$$\frac{\Delta\omega_{12}^*}{k_{\text{esc}}} \simeq -\frac{1}{4} \left(t + \frac{1}{1 - e^{-\frac{1}{2}\omega_{\text{tot}}}} \right). \quad (18)$$

See SI: Processivity for derivations. In Fig. 4, Eqs. 17 and 18 (thick black dotted curves) closely match the numerical $\Delta\omega_{12}^*/k_{\text{esc}}$ (solid and dashed curves) for low k_{esc} and low t .

For high free energy budget ω_{tot} , the allocation ω_{12}^* in Fig. 4 is intuitive: ω_{12}^* is low and (although not shown in the figure) $\omega_{21}^* = \omega_{\text{tot}} - \omega_{12}^*$ is high, reducing the probability of being in the vulnerable state 2. For higher escape rates and longer times, the difference $|\Delta\omega_{ij}^*|$ between optimal and naive allocations increases, diverging as time $t \rightarrow \infty$.

In Fig. 4, $\Delta\omega_{12}^*$ for FL changes sign from negative to positive as ω_{tot} decreases, with the change occurring at larger ω_{tot} for shorter times. Positive $\Delta\omega_{12}^*$ increases the probability in the vulnerable state and increases the escape rate. But maximizing Φ_{acc} is a tradeoff between reducing escape and increasing ongoing flux. For longer times t and higher ω_{tot} , it is more important to reduce escape to preserve the future flux, and the intuitive result ($\Delta\omega_{12}^* < 0$) is observed. However, at small t and ω_{tot} , initial flux is relatively more important, as little escape occurs before time t is reached. The escaping flux from state 2 causes $P_1 > P_2$ for naive free energy allocation $\omega_{12} = \omega_{21} = \frac{1}{2}\omega_{\text{tot}}$. FL only allows the forward fluxes to be increased — to maximize the flux, the forward flux for transition 12 should be increased more, because $P_1 > P_2$, leading to $\Delta\omega_{12}^* > 0$. In contrast, RL only allows reverse fluxes to be decreased — to maximize the flux, the reverse flux for transition 21 should be decreased more, again because $P_1 > P_2$, consistently leading to $\Delta\omega_{12}^* < 0$.

Discussion

Biomolecular machines perform a variety of tasks inside cells, driven by the free energy stored in intracellular chemical concentrations. Here we investigated how to maximize flux in molecular machines with multiple free energy components, and how to maintain processivity.

Central to our approach is the general manner in which forward and reverse rate constants are affected by free energy changes.^{11,12,26} Free energy components that only affect the forward or reverse rate constants represent extremes, and the division of the effect of free energy components between the forward and reverse rate constants is more generally described by a splitting factor $\delta \in [0, 1]$. We primarily consider the simplifying case where splitting factors for all distinct free energy components are equal.

In contrast with previous results,¹² we find no single splitting factor δ generally maximizes the flux. Instead, the optimal splitting factor depends on the detailed free energy allocation, with flux decreasing significantly away from the optimal splitting factor (Fig. 2).

Previous studies^{11,12} argued that low splitting factors are optimal, suggesting low splitting factors would describe the operation of evolved biomolecular machines. We have shown that both low and high splitting factors can maximize flux, and that the optimal splitting factor value depends on the allocation of free energy. Experimental fits of splitting factors find both low splitting factors^{11,19,34–36} and high splitting factors.^{35,37} These fits use several models for the dependence of rate constants on resisting forces.^{11,19,34–38} Unlike in our model, all other models we have found assume that rate constants only explicitly contain splitting factors for force, with no splitting factors for other free energy components (though one other model has implicit splitting of the effect of chemical potential¹¹). Splitting factor analysis has largely been done in the context of ‘canonical’ molecular machines, such as the walking motors kinesin,^{35–38} myosin,^{11,19} and dynein,³⁹ or the rotary motor F1-ATPase.³⁴ Splitting factors δ are not always robust, with distinct data sets for kinesin motility^{40,41} leading to substantially different inferred values of 0.3 and 0.65.³⁷ It would be an interesting follow up to investigate splitting factors for all free energy components affecting rate constants, and for a broader class of molecular machines, which may lead to a broader diversity of splitting factor values. In SI: Experimental splitting factors, we describe in more detail the fitted splitting factors for various models.^{11,19,34–38}

Flux can also be maximized by varying free energy components ω_{ij}^k , with flux significantly decreasing away from the optimal ω_{ij}^{k*} . For a scenario with two distinct free energy components, one variable and one fixed, the flux is maximized by allocating the variable free energy component to compensate for any departure from optimal of the fixed free energy component allocation. There are examples of machine models fit to experimental data where transitions with a fixed load appear to receive more of the other free energy components than those without a load (consistent with our predictions),^{1,35,36} but also counter-examples that do not fit this optimal framework.^{19,38}

Through mutation, biomolecular machine operation can change, and we expect evolution to select machine parameters that favor certain performance characteristics. We argue that robustness increases when tuning parameters to maximize flux with a load, rather than without a load, because for load-optimized parameters the flux is less sensitive to the presence or absence of load. This is consistent with observations of kinesin maintaining a stable velocity under a range of forces,⁴² an intuitively beneficial trait.⁴³

We also examined cycles that are transiently processive and escape from a single vulnerable state. For large free energy budgets, maximizing the number of complete cycles before the cycle escapes leads to intuitive allocations: free energy is primarily allocated to decrease the probability present in the vulnerable state. However, for small free energy budgets, to maximize the number of cycles completed, free energy is primarily allocated to increase the flux — for forward labile cycles this increases the probability present in the vulnerable state, while for reverse labile cycles this decreases it. Although this forward labile allocation increases the rate of escape, the associated flux increase more than compensates,

leading to an overall increase in the accumulated flux.

Kinesins mutated to have different neck linker charge show increased processivity, which is attributed to shorter waiting times in states vulnerable to detachment from the microtubule.^{29,32,44} These findings are consistent with our result that occupation of the vulnerable state be reduced to maximize processivity for large free energy budgets, such as the $\sim 20k_B T$ of free energy from ATP hydrolysis²¹ driving each kinesin cycle.⁴⁵

While we are unaware of other modeling that maximizes processivity, Hill modeled escape as a transition to the initial state where all trajectories begin, effectively acting as an additional subcycle.⁴⁶ This steady state with immediate rebinding is distinct from our steady state without rebinding. Both Hill's approach and ours allow calculation of detachment rates (distinct due to differing steady states); but our approach additionally quantifies progress before detachment.

Acknowledgement

This work was supported by a Natural Sciences and Engineering Research Council of Canada (NSERC) Discovery Grant, by funds provided by the Faculty of Science, Simon Fraser University through the President's Research Start-up Grant, by a Tier II Canada Research Chair, and by WestGrid (www.westgrid.ca) and Compute Canada Calcul Canada (www.computeCanada.ca). The authors thank Emma Lathouwers and Steven Large (SFU Physics) for useful discussions and feedback.

Supplemental Information

Maximizing flux: Varying splitting factors

Free energy components ω_{ij}^k influence the forward and reverse rate constants, parameterized by δ_{ij}^k ,

$$k_{ij}^+ = k_{ij}^0 e^{\sum_k \delta_{ij}^k \sigma_{ij}^k} \quad \text{and} \quad k_{ij}^- = k_{ij}^0 e^{-\sum_k (1-\delta_{ij}^k) \omega_{ij}^k} . \quad (\text{S1})$$

In the main text we showed that if $\delta_{ij}^k = \delta$, there is no value of δ that generally maximizes the flux. The results of this section, with no consistent sign for $\partial J / \partial \delta_{12}^I$, $\partial J / \partial \delta^I$, and $\partial J / \partial \delta_{12}$, similarly conclude that there are no generally optimal values for δ_{ij}^k . Having no general optimal δ_{ij}^k value does not align with previous results¹² where the power of a motor was maximized for a power stroke ($\delta = 0$).

The two-state cycle steady-state flux is

$$J = \frac{k_{12}^+ k_{21}^+ - k_{12}^- k_{21}^-}{k_{12}^+ + k_{12}^- + k_{21}^+ + k_{21}^-} . \quad (\text{S2})$$

For the cases below we consider two free energy components, ω^I and ω^{II} , subject to the relationships $\omega_{\text{tot}}^I = \sum \omega_{ij}^I$, $\omega_{\text{tot}}^{II} = \sum \omega_{ij}^{II}$, and $\omega_{\text{tot}} = \omega_{\text{tot}}^I + \omega_{\text{tot}}^{II}$.

Case 1

In this case, we allow the splitting constants to differ between transitions, but require equality for different free energy components, $\delta_{ij}^k = \delta_{ij}$. This gives flux

$$J = \frac{k_{12}^0 k_{21}^0 (1 - e^{-\omega_{\text{tot}}})}{k_{12}^0 e^{-\delta_{21} \omega_{21}} (1 + e^{-\omega_{12}}) + k_{21}^0 e^{-\delta_{12} \omega_{12}} (1 + e^{-\omega_{21}})} . \quad (\text{S3})$$

The flux increases with increasing δ_{12} as

$$\frac{\partial J}{\partial \delta_{12}} = \frac{k_{12}^0 (k_{21}^0)^2 \omega_{12} (1 - e^{-\omega_{\text{tot}}}) e^{-\delta_{12} \omega_{12}} (1 + e^{-\omega_{21}})}{[k_{12}^0 e^{-\delta_{21} \omega_{21}} (1 + e^{-\omega_{12}}) + k_{21}^0 e^{-\delta_{12} \omega_{12}} (1 + e^{-\omega_{21}})]^2}. \quad (\text{S4})$$

The flux is maximized for $\delta_{12} = 0$ if $\omega_{12} < 0$ and for $\delta_{12} = 1$ if $\omega_{12} > 0$. Variation of δ_{21} produces a similar result.

Case 2

If we allow the splitting constants to differ for different free energy components, but not between transitions, so that $\delta_{ij}^I = \delta^I$ and $\delta_{ij}^{II} = \delta^{II}$ in Eq. S1, the flux and its derivative are

$$J = \frac{k_{12}^0 k_{21}^0 (1 - e^{-\omega_{\text{tot}}})}{k_{12}^0 e^{-\delta^I \omega_{21}^I - \delta^{II} \omega_{21}^{II}} (1 + e^{-\omega_{12}}) + k_{21}^0 e^{-\delta^I \omega_{12}^I - \delta^{II} \omega_{12}^{II}} (1 + e^{-\omega_{21}})}. \quad (\text{S5a})$$

$$\frac{\partial J}{\partial \delta^I} = \frac{k_{12}^0 k_{21}^0 (1 - e^{-\omega_{\text{tot}}}) \left[k_{12}^0 \omega_{21}^I e^{-\delta^I \omega_{21}^I - \delta^{II} \omega_{21}^{II}} (1 + e^{-\omega_{12}}) + k_{21}^0 \omega_{12}^I e^{-\delta^I \omega_{12}^I - \delta^{II} \omega_{12}^{II}} (1 + e^{-\omega_{21}}) \right]}{\left[k_{12}^0 e^{-\delta^I \omega_{21}^I - \delta^{II} \omega_{21}^{II}} (1 + e^{-\omega_{12}}) + k_{21}^0 e^{-\delta^I \omega_{12}^I - \delta^{II} \omega_{12}^{II}} (1 + e^{-\omega_{21}}) \right]^2}. \quad (\text{S5b})$$

If $\omega_{12}^I > 0$ and $\omega_{21}^I > 0$ then $\partial J / \partial \delta^I > 0$, and $\delta^I = 1$ maximizes the flux. However, both ω_{12}^I and ω_{21}^I are not always positive, so $\partial J / \partial \delta^I$ is not always positive or negative, with the flux maximized for

$$\delta^I = \frac{1}{\omega_{21}^I - \omega_{12}^I} \left\{ \delta^{II} (\omega_{12}^{II} - \omega_{21}^{II}) + \ln \left[\frac{-\omega_{21}^I k_{12}^0 (1 + e^{-\omega_{12}})}{\omega_{12}^I k_{21}^0 (1 + e^{-\omega_{21}})} \right] \right\}. \quad (\text{S6})$$

Similar results are found for variation of δ^{II} .

Case 3

The most general case has splitting constants varying between transitions and between free energy components, as in Eq. S1, giving

$$J = \frac{k_{12}^0 k_{21}^0 (1 - e^{-\omega_{\text{tot}}})}{k_{12}^0 e^{-\delta_{21}^I \omega_{21}^I - \delta_{21}^{II} \omega_{21}^{II}} (1 + e^{-\omega_{12}}) + k_{21}^0 e^{-\delta_{12}^I \omega_{12}^I - \delta_{12}^{II} \omega_{12}^{II}} (1 + e^{-\omega_{21}})}, \quad (\text{S7a})$$

$$\frac{\partial J}{\partial \delta_{12}^I} = \frac{k_{12}^0 (k_{21}^0)^2 \omega_{12}^I (1 - e^{-\omega_{\text{tot}}}) e^{-\delta_{12}^I \omega_{12}^I - \delta_{12}^{II} \omega_{12}^{II}} (1 + e^{-\omega_{21}})}{\left[k_{12}^0 e^{-\delta_{21}^I \omega_{21}^I - \delta_{21}^{II} \omega_{21}^{II}} (1 + e^{-\omega_{12}}) + k_{21}^0 e^{-\delta_{12}^I \omega_{12}^I - \delta_{12}^{II} \omega_{12}^{II}} (1 + e^{-\omega_{21}}) \right]^2}. \quad (\text{S7b})$$

If $\omega_{12}^I > 0$, then $\partial J / \partial \delta_{12}^I > 0$, leading to $\delta_{12}^I = 1$ maximizing flux; conversely $\omega_{12}^I < 0$ leads to $\delta_{12}^I = 0$ maximizing flux. Similar results are found for variation of δ_{21}^I , δ_{12}^{II} , and δ_{21}^{II} .

Maximizing flux: Varying free energy

Here we examine what free energy allocation ω_{ij} (composed of free energy components ω_{ij}^k) maximizes the flux. We go through distinct cases for splitting the effect of two free energy components between forward and reverse rate constants. In the main text, we find that for free energy components split identically across all transitions ($\delta_{ij}^I = \delta_{ij}^{II} = \delta$), there is no closed form for the optimal free energy allocation ω_{ij}^* , but that for $\delta = 0$ or $\delta = 1$, closed forms can be found. We review these results below, as well as other splitting scenarios with similar results.

Case 1

Here both free energy components are split identically across all transitions, $\delta_{ij}^I = \delta_{ij}^{II} = \delta$, giving rate constants

$$k_{ij}^+ = k_{ij}^0 e^{\delta\omega_{ij}} \quad \text{and} \quad k_{ij}^- = k_{ij}^0 e^{-(1-\delta)\omega_{ij}} . \quad (\text{S8})$$

The flux and its derivative are

$$J = \frac{k_{12}^0 k_{21}^0 e^{\delta\omega_{\text{tot}}} (1 - e^{-\omega_{\text{tot}}})}{k_{12}^0 e^{\delta\omega_{12}} (1 + e^{-\omega_{12}}) + k_{21}^0 e^{\delta(\omega_{\text{tot}} - \omega_{12})} (1 + e^{-(\omega_{\text{tot}} - \omega_{12})})} , \quad (\text{S9a})$$

$$\frac{\partial J}{\partial \omega_{12}} = \frac{-k_{12}^0 k_{21}^0 e^{\delta\omega_{\text{tot}}} (1 - e^{-\omega_{\text{tot}}}) \{k_{12}^0 e^{\delta\omega_{12}} [\delta - (1 - \delta)e^{-\omega_{12}}] + k_{21}^0 e^{\delta(\omega_{\text{tot}} - \omega_{12})} [-\delta + (1 - \delta)e^{-(\omega_{\text{tot}} - \omega_{12})}]\}}{[k_{12}^0 e^{\delta\omega_{12}} (1 + e^{-\omega_{12}}) + k_{21}^0 e^{\delta(\omega_{\text{tot}} - \omega_{12})} (1 + e^{-(\omega_{\text{tot}} - \omega_{12})})]^2} . \quad (\text{S9b})$$

Setting $\partial J / \partial \omega_{12} = 0$ yields

$$k_{12}^0 e^{\delta\omega_{12}^*} [\delta - (1 - \delta)e^{-\omega_{12}^*}] = k_{21}^0 e^{\delta(\omega_{\text{tot}} - \omega_{12}^*)} [\delta - (1 - \delta)e^{-(\omega_{\text{tot}} - \omega_{12}^*)}] . \quad (\text{S10})$$

Case 2

For this case two free energy components are split differently, but the splitting is the same for all transitions. The rate constants are then

$$k_{ij}^+ = k_{ij}^0 e^{\delta^I \omega_{ij}^I + \delta^{II} \omega_{ij}^{II}} \quad \text{and} \quad k_{ij}^- = k_{ij}^0 e^{-(1-\delta^I)\omega_{ij}^I - (1-\delta^{II})\omega_{ij}^{II}} . \quad (\text{S11})$$

The flux and its derivative are

$$J = \frac{k_{12}^0 k_{21}^0 e^{\delta^I \omega_{\text{tot}}^I + \delta^{II} \omega_{\text{tot}}^{II}} (1 - e^{-\omega_{\text{tot}}})}{\{k_{12}^0 e^{\delta^I \omega_{12}^I + \delta^{II} \omega_{12}^{II}} (1 + e^{-\omega_{12}}) + k_{21}^0 e^{\delta^I (\omega_{\text{tot}}^I - \omega_{12}^I) + \delta^{II} (\omega_{\text{tot}}^{II} - \omega_{12}^{II})} (1 + e^{-(\omega_{\text{tot}} - \omega_{12})})\}} , \quad (\text{S12a})$$

$$\frac{\partial J}{\partial \omega_{12}^I} = \frac{-k_{12}^0 k_{21}^0 e^{\delta^I \omega_{\text{tot}}^I + \delta^{II} \omega_{\text{tot}}^{II}} (1 - e^{-\omega_{\text{tot}}}) \left\{ \begin{array}{l} k_{12}^0 e^{\delta^I \omega_{12}^I + \delta^{II} \omega_{12}^{II}} [\delta^I - (\delta^I - 1)e^{-\omega_{12}}] + \\ k_{21}^0 e^{\delta^I (\omega_{\text{tot}}^I - \omega_{12}^I) + \delta^{II} (\omega_{\text{tot}}^{II} - \omega_{12}^{II})} [-\delta^I + (1 - \delta^I)e^{-(\omega_{\text{tot}} - \omega_{12})}] \end{array} \right\}}{\{k_{12}^0 e^{\delta^I \omega_{12}^I + \delta^{II} \omega_{12}^{II}} (1 + e^{-\omega_{12}}) + k_{21}^0 e^{\delta^I (\omega_{\text{tot}}^I - \omega_{12}^I) + \delta^{II} (\omega_{\text{tot}}^{II} - \omega_{12}^{II})} (1 + e^{-(\omega_{\text{tot}} - \omega_{12})})\}^2} . \quad (\text{S12b})$$

Case 3

For this case, different free energy components are split the same, but the splitting is different for each transition. The rate constants are then

$$k_{ij}^+ = k_{ij}^0 e^{\delta_{ij}\omega_{ij}} \quad \text{and} \quad k_{ij}^- = k_{ij}^0 e^{-(1-\delta_{ij})\omega_{ij}} . \quad (\text{S13})$$

The flux and its derivative are

$$J = \frac{k_{12}^0 k_{21}^0 (1 - e^{-\omega_{\text{tot}}})}{[k_{12}^0 e^{-\delta_{21}(\omega_{\text{tot}} - \omega_{12})} (1 + e^{-\omega_{12}}) + k_{21}^0 e^{-\delta_{12}\omega_{12}} (1 + e^{-(\omega_{\text{tot}} - \omega_{12})})]} , \quad (\text{S14a})$$

$$\frac{\partial J}{\partial \omega_{12}} = \frac{-k_{12}^0 k_{21}^0 (1 - e^{-\omega_{\text{tot}}}) \left\{ \begin{array}{l} k_{12}^0 e^{-\delta_{21}(\omega_{\text{tot}} - \omega_{12})} [\delta_{21} + (\delta_{21} - 1)e^{-\omega_{12}}] - \\ k_{21}^0 e^{-\delta_{12}\omega_{12}} [\delta_{12} + (\delta_{12} - 1)e^{-(\omega_{\text{tot}} - \omega_{12})}] \end{array} \right\}}{[k_{12}^0 e^{-\delta_{21}(\omega_{\text{tot}} - \omega_{12})} (1 + e^{-\omega_{12}}) + k_{21}^0 e^{-\delta_{12}\omega_{12}} (1 + e^{-(\omega_{\text{tot}} - \omega_{12})})]^2} . \quad (\text{S14b})$$

Case 4

For this case, different free energy components are split differently, and the splitting is different for each transition. The rate constants are then

$$k_{ij}^+ = k_{ij}^0 e^{\delta_{ij}^I \omega_{ij}^I + \delta_{ij}^{II} \omega_{ij}^{II}} \quad \text{and} \quad k_{ij}^- = k_{ij}^0 e^{-(1-\delta_{ij}^I) \omega_{ij}^I - (1-\delta_{ij}^{II}) \omega_{ij}^{II}}. \quad (\text{S15})$$

The flux and its derivative are

$$J = \frac{k_{12}^0 k_{21}^0 (1 - e^{-\omega_{\text{tot}}})}{k_{12}^0 e^{-\delta_{21}^I (\omega_{\text{tot}}^I - \omega_{12}^I) - \delta_{21}^{II} (\omega_{\text{tot}}^{II} - \omega_{12}^{II})} (1 + e^{-\omega_{12}}) + k_{21}^0 e^{-\delta_{12}^I \omega_{12}^I - \delta_{12}^{II} \omega_{12}^{II}} (1 + e^{-(\omega_{\text{tot}} - \omega_{12})})}, \quad (\text{S16a})$$

$$\frac{\partial J}{\partial \omega_{12}^I} = \frac{-k_{12}^0 k_{21}^0 (1 - e^{-\omega_{\text{tot}}^I - \omega_{\text{tot}}^{II}}) \left\{ \begin{array}{l} k_{12}^0 e^{-\delta_{21}^I (\omega_{\text{tot}}^I - \omega_{12}^I) - \delta_{21}^{II} (\omega_{\text{tot}}^{II} - \omega_{12}^{II})} [\delta_{21}^I + (\delta_{21}^I - 1) e^{-\omega_{12}}] - \\ k_{21}^0 e^{-\delta_{12}^I \omega_{12}^I - \delta_{12}^{II} \omega_{12}^{II}} [\delta_{12}^I + (\delta_{12}^I - 1) e^{-(\omega_{\text{tot}} - \omega_{12})}] \end{array} \right\}}{[k_{12}^0 e^{-\delta_{21}^I (\omega_{\text{tot}}^I - \omega_{12}^I) - \delta_{21}^{II} (\omega_{\text{tot}}^{II} - \omega_{12}^{II})} (1 + e^{-\omega_{12}}) + k_{21}^0 e^{-\delta_{12}^I \omega_{12}^I - \delta_{12}^{II} \omega_{12}^{II}} (1 + e^{-(\omega_{\text{tot}} - \omega_{12})})]^2}. \quad (\text{S16b})$$

Case 1 is considered in the main text, while cases 2-4 are not. A closed form for ω_{12}^* (when splitting factors are equal for different free energy components) or ω_{12}^{I*} (when they are not) solving $\partial J / \partial \omega_{12} = 0$ or $\partial J / \partial \omega_{12}^I = 0$, respectively, cannot generally be found for any of these cases. We now consider some simplifying cases, with one or both of splitting factors δ^I and δ^{II} set to the extremes 0 or 1, to arrive at some closed-form solutions for ω_{12}^* .

Case 5

For this case, all free energy components split the same, and the splitting is the same for each transition, with splitting factor $\delta = 1$, corresponding to forward labile. Setting $\delta = 1$ in Eq. S10 gives the flux-maximizing free energy allocation

$$\omega_{12}^* = \frac{1}{2} \omega_{\text{tot}} + \frac{1}{2} \ln \frac{k_{21}^0}{k_{12}^0}. \quad (\text{S17})$$

This corresponds to

$$\omega_{12}^{I*} = -\omega_{12}^{II*} + \frac{1}{2} \omega_{\text{tot}} + \frac{1}{2} \ln \frac{k_{21}^0}{k_{12}^0}. \quad (\text{S18})$$

Case 6

For this case, all free energy components split the same, and the splitting is the same for each transition, with splitting factor $\delta = 0$ corresponding to reverse labile. Setting $\delta = 0$ in Eq. S10 gives the flux-maximizing free energy allocation

$$\omega_{12}^* = \frac{1}{2} \omega_{\text{tot}} - \frac{1}{2} \ln \frac{k_{21}^0}{k_{12}^0}. \quad (\text{S19})$$

This corresponds to

$$\omega_{12}^{I*} = -\omega_{12}^{II*} + \frac{1}{2} \omega_{\text{tot}} - \frac{1}{2} \ln \frac{k_{21}^0}{k_{12}^0}. \quad (\text{S20})$$

For cases 5 and 6 the flux-maximizing allocation of ω^I compensates exactly for ω^{II} on each transition, and uses the remaining free energy to maximize the flux as if $\omega^{II} = 0$.

Experimental splitting factors

Table S1 summarizes splitting factors derived from fits to experimental data.

Table S1: Splitting factors from experimental fits. Splitting factors δ fit to data from a variety of molecular machines, arranged in order of range midpoints.

| δ range | Model | Machine |
|----------------|---------|-------------------------------------|
| 0.004 – 0.024 | Eq. S21 | Myosin ¹¹ |
| –0.03 – 0.08 | Eq. S24 | Myosin ¹⁹ |
| 0 – 0.13 | Eq. S24 | Kinesin ³⁶ |
| 0.1 – 0.3 | Eq. S22 | F ₁ ATPase ³⁴ |
| 0.04 – 0.48 | Eq. S24 | Kinesin (four-state) ³⁵ |
| 0.04 – 0.62 | Eq. S24 | Kinesin (two-state) ³⁵ |
| 0.3 – 0.65 | Eq. S23 | Kinesin ³⁷ |
| 0.04 – 2.8 | Eq. S24 | Kinesin ³⁸ |

In Schmiedl and Seifert¹¹ a discrete-state model has rate constants

$$k^+ = k^0 e^{\Delta\mu^+ - \beta\delta Fd} , \quad (\text{S21a})$$

$$k^- = k^0 e^{-\Delta\mu^- + \beta(1-\delta)Fd} . \quad (\text{S21b})$$

Their δ are identical to our splitting factors. For a two-state myosin model, they find $\delta_{12} = 0.004$ and $\delta_{21} = 0.024$.

Zimmermann and Seifert³⁴ model a continuous free energy landscape with forward and reverse rate constants

$$k^+(n, x) = k^0 e^{\Delta\mu_{\text{ATP}} - \kappa d \delta (d\delta/2 + n - x)} , \quad (\text{S22a})$$

$$k^-(n, x) = k^0 e^{\Delta\mu_{\text{ADP}} + \Delta\mu_{\text{P}_i} - \kappa d (1-\delta) [d(1-\delta)/2 - n + x]} . \quad (\text{S22b})$$

d is motor step size, κ is the spring constant between the motor and attached probe, and $\Delta\mu_i = \mu_i - \mu_i^{\text{eq}} = \ln c_i/c_i^{\text{eq}}$ are the chemical potential differences from equilibrium. Rate constants $k^{+/-}$ and k^0 do not have indices because the model contains only one step. Splitting factor δ is found by fitting to experimental F₁ ATPase data.

In Liepelt and Lipowsky³⁷ a discrete-state model has rate constants

$$k_{ij} = k_{ij}^0 \Phi(F) . \quad (\text{S23})$$

For chemical transitions, $\Phi_{ij}(F) = \Phi_{ji}(F) = 2/[1 + e^{\chi_{ij}F/k_{\text{B}}T}]$, with χ_{ij} a dimensionless force parameter similar to δ or θ . For mechanical transitions, $\Phi(F) = e^{-\delta F}$ for the direction against the load, and $\Phi(F) = e^{(1-\delta)F}$ for the opposite direction. Using distinct kinesin motility data sets,^{40,41} they find $\delta = 0.3$ or 0.6 .

Fisher and Kolomeisky³⁵ construct a discrete-state model with forward and reverse rate constants

$$k_{ij}^+ = k_{ij}^{+0} e^{-\theta_{ij}^+ Fd} , \quad (\text{S24a})$$

$$k_{ij}^- = k_{ij}^{-0} e^{\theta_{ij}^- Fd} . \quad (\text{S24b})$$

F is a constant opposing force, d is the motor step over a complete cycle, and $k_{ij}^{\pm 0}$ are the rate constants at zero force. The $\theta_{ij}^{+/-}$ are found by fitting to experimental kinesin data, but are not identical to our splitting factors δ_{ij} . Instead, they use the constraint $\sum(\theta_{ij}^+ + \theta_{ij}^-) = 1$, such that $\theta_{ij}^{+/-}$ is a combination of allocating a load to the various transitions and splitting the impact of the load between the forward

and reverse rate constants. For a two-state model, for the first transition, they find $\theta_{12}^+ = 0.135$ and $\theta_{12}^- = 0.08$, equivalent to $\delta_{12} = 0.62$. For the second transition, they find $\theta_{21}^+ = 0.035$ and $\theta_{21}^- = 0.75$, equivalent to $\delta_{21} = 0.04$. For a four-state model, the first transition is found to have $\theta_{12}^+ = 0.12$ and $\theta_{12}^- = 0.13$ ($\delta_{12} = 0.48$), the second transition $\theta_{23}^+ = 0.02$ and $\theta_{23}^- = 0.13$ ($\delta_{23} = 0.13$), the third transition $\theta_{34}^+ = 0.02$ and $\theta_{34}^- = 0.13$ ($\delta_{34} = 0.13$), and the fourth transition $\theta_{41}^+ = 0.02$ and $\theta_{41}^- = 0.43$ ($\delta_{41} = 0.04$). The second transition of the two-state model, and the fourth transition of the four-state model, are treated as the most irreversible, indicating these transitions are allocated the most free energy. These transitions are also fit with the largest θ values, so that more of the other free energy components are allocated to transitions with more load. A later publication by the same authors,¹⁹ with a two-state myosin model using the same force dependence, fitted the first transition with $\theta_{12}^+ = -0.01$ and $\theta_{12}^- = 0.385$ ($\delta_{12} = -0.03$) and a second transition with $\theta_{21}^+ = 0.045$ and $\theta_{21}^- = 0.58$ ($\delta_{21} = 0.08$). In this case, the second transition is fit with a greater load, but is not allocated a greater amount of other free energy components.

In Hwang and Hyeon,³⁶ a discrete-state model for kinesin has forward and reverse rate constants with the same force dependence as Eq. S24. With four states, the first transition is fit with $\theta_{12}^+ = 0$ and $\theta_{12}^- = 0.15$ ($\delta_{12} = 0$), the second transition with $\theta_{23}^+ = 0.04$ and $\theta_{23}^- = 0.5$ ($\delta_{23} = 0.07$), the third transition with $\theta_{34}^+ = 0.01$ and $\theta_{34}^- = 0.14$ ($\delta_{34} = 0.07$), and the fourth transition with $\theta_{41}^+ = 0.02$ and $\theta_{41}^- = 0.14$ ($\delta_{41} = 0.125$). The second transition is fit with the largest load (high θ values) and has a larger amount of the other free energy components.

In Lau *et al.*,³⁸ a discrete-state model for kinesin has forward and reverse rate constants with the same force dependence as Eq. S24. With two states, the first transition is fitted with $\theta_{12}^+ = 0.25$ and $\theta_{12}^- = -0.16$ ($\delta_{12} = 2.8$) and the second transition with $\theta_{21}^+ = 0.08$ and $\theta_{21}^- = 1.83$ ($\delta_{21} = 0.04$). These are fit with the constraint $\theta_{12}^+ + \theta_{12}^- + \theta_{21}^+ + \theta_{21}^- = 2$. The transition state picture (*e.g.* in Schmiedl and Seifert¹¹) describes an opposing force as reducing the rate of forward transitions and/or increasing the rate of reverse transitions. This transition state picture does not explain the $\theta_{ij}^{+/-}$ values in Lau *et al.*³⁸ because for transition 12 both the forward and reverse transition rates are decreased by opposing force.

Processivity

Two states

With state 2 vulnerable to escape, the governing differential equations are

$$\frac{dP_1}{dt} = -(k_{12}^+ + k_{21}^-)P_1 + (k_{12}^- + k_{21}^+)P_2 \quad (\text{S25a})$$

$$\frac{dP_2}{dt} = (k_{12}^+ + k_{21}^-)P_1 - (k_{12}^- + k_{21}^+)P_2 - k_{\text{esc}}P_2. \quad (\text{S25b})$$

We rewrite these differential equations in terms of P_i/P_{tot} , where $P_{\text{tot}}(t) = P_1(t) + P_2(t)$ is the total remaining probability that has not yet escaped the cycle. Using

$$\frac{d\left(\frac{P_i}{P_{\text{tot}}}\right)}{dt} = \frac{1}{P_{\text{tot}}} \frac{dP_i}{dt} - \frac{P_i}{P_{\text{tot}}^2} \frac{dP_{\text{tot}}}{dt}, \quad (\text{S26})$$

and $dP_{\text{tot}}/dt = -k_{\text{esc}}P_2$, gives

$$\frac{d\left(\frac{P_1}{P_{\text{tot}}}\right)}{dt} = -(k_{12}^+ + k_{21}^-) \frac{P_1}{P_{\text{tot}}} + (k_{12}^- + k_{21}^+) \frac{P_2}{P_{\text{tot}}} + k_{\text{esc}} \frac{P_1}{P_{\text{tot}}} \frac{P_2}{P_{\text{tot}}}. \quad (\text{S27})$$

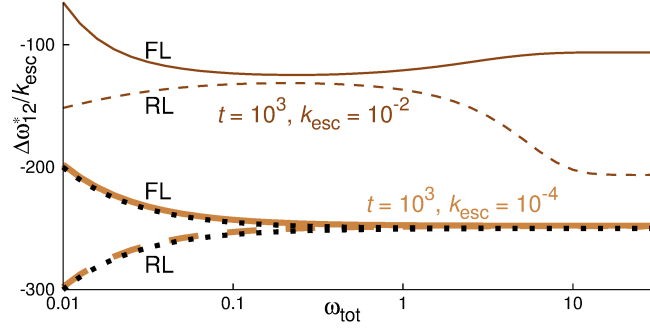


Figure S1: **Non-monotonic optimal free energy allocation reflects competition between flux and avoiding escape.** Free energy allocation ω_{ij} that maximizes accumulated flux Φ_{acc} (Eq. 16) for $t = 1000$, in two-state cycle with $k_{12}^0 = k_{21}^0 = 1$ and variable escape rate k_{esc} . FL plotted as solid lines, RL as dashed lines. Thick black dotted curves show Eqs. 17 and 18, which approximate $\Delta\omega_{12}^*/k_{\text{esc}}$ for low k_{esc} . Allocation is shown as the difference $\Delta\omega_{ij}^* = \omega_{ij}^* - \frac{1}{2}\omega_{\text{tot}}$ from the ‘naive’ equal allocation $\frac{1}{2}\omega_{\text{tot}}$ to each transition. $\Delta\omega_{21}^* = -\Delta\omega_{12}^*$ is not shown. Initial condition is the steady state for P_i/P_{tot} .

Substituting $\frac{P_1}{P_{\text{tot}}} = 1 - \frac{P_2}{P_{\text{tot}}}$ into Eq. S27 at steady state (when $d(P_i/P_{\text{tot}})/dt = 0$) gives a quadratic equation for P_2/P_{tot} :

$$k_{\text{esc}} \left(\frac{P_2}{P_{\text{tot}}} \right)^2 - [k_{12}^+ + k_{12}^- + k_{21}^+ + k_{21}^- + k_{\text{esc}}] \left(\frac{P_2}{P_{\text{tot}}} \right) + k_{12}^+ + k_{21}^- = 0. \quad (\text{S28})$$

P_2/P_{tot} has a real solution when the discriminant is non-negative.

Optimizing two-state flux accumulated over large t

Fig. 4 shows that for small k_{esc} and t , $\Delta\omega_{12}^*$ changes monotonically as ω_{tot} increases. However, for $k_{\text{esc}} = 10^{-2}$ and $t = 1000$, $\Delta\omega_{12}^*$ is non-monotonic (Fig. S1). As mentioned in the main text, the accumulated flux Φ_{acc} is the integrated flux over a period of time, and reflects both the instantaneous flux and escape from state 2. Increasing ω_{tot} shifts the respective functional dependences of flux and P_2/P_{tot} on ω_{12} , often in ways producing competing influences on $\Delta\omega_{12}^*$. For sufficiently high ω_{tot} , the functional dependences asymptote to forms that don’t change with further increased ω_{tot} . For small t and k_{esc} , these functional dependences cease changing at approximately the same high value of ω_{tot} , leading $\Delta\omega_{12}^*$ to be monotonic in ω_{tot} in Fig. 4. However for larger t and k_{esc} , the functional dependences cease changing at different values of ω_{tot} . Since the (potentially countervailing) influences on $\Delta\omega_{12}^*$ do not happen over the same ω_{tot} range, $\Delta\omega_{12}^*$ can change non-monotonically with ω_{tot} , as seen for $t = 10^3$ and $k_{\text{esc}} = 10^{-2}$ in Fig. S1.

For $k_{\text{esc}} = 10^{-2}$ and $t = 1000$ (Fig. S1), $\Delta\omega_{12}^*$ for FL and RL do not coincide at high ω_{tot} . This distinction between FL and RL at high ω_{tot} occurs because with more free energy dissipation, FL increases rate constants while RL decreases rate constants. At high ω_{tot} , the rate constants for FL can still significantly change with more ω_{ij} , while the rate constants for RL are already quite small. This leads RL to require a larger $|\Delta\omega_{12}^*|$ than FL. This effect also occurs for lower k_{esc} and t in Fig. 4, but is much smaller because escape rates and/or total probability escaping is much smaller.

Two-state optimization approximation for low k_{esc} , t

Equations 17 and 18 are approximations for the free energy allocation $\Delta\omega_{12}^*$ that maximize the accumulated flux for small k_{esc} and t .

We first derive Eq. 17 for FL rate constants with $k_{12}^0 = k_{21}^0 = 1$, $k_{12}^+ = e^{\omega_{\text{tot}}/2} e^{\Delta\omega_{12}}$, and $k_{21}^+ = e^{\omega_{\text{tot}}/2} e^{-\Delta\omega_{12}}$, beginning with Eq. S28 and solving for P_2 using the quadratic formula,

$$\frac{P_2}{P_{\text{tot}}} = (e^{\omega_{\text{tot}}/2} e^{\Delta\omega_{12}} + e^{\omega_{\text{tot}}/2} e^{-\Delta\omega_{12}} + 2 + k_{\text{esc}}) \left(1 - \sqrt{1 - \frac{4k_{\text{esc}}(e^{\omega_{\text{tot}}/2} e^{\Delta\omega_{12}} + 1)}{(e^{\omega_{\text{tot}}/2} e^{\Delta\omega_{12}} + e^{\omega_{\text{tot}}/2} e^{-\Delta\omega_{12}} + 2 + k_{\text{esc}})^2}} \right). \quad (\text{S29})$$

Taylor expanding for small k_{esc} and $\Delta\omega_{12}$ gives

$$\frac{P_2}{P_{\text{tot}}} \simeq \frac{1}{2} \left[1 + \frac{\Delta\omega_{12}}{1 + e^{-\omega_{\text{tot}}/2}} - \frac{k_{\text{esc}}}{4(1 + e^{\omega_{\text{tot}}/2})} \right]. \quad (\text{S30})$$

The flux is

$$J_{12} + J_{21} = e^{\omega_{\text{tot}}/2} e^{\Delta\omega_{12}} \frac{P_1}{P_{\text{tot}}} - \frac{P_2}{P_{\text{tot}}} + e^{\omega_{\text{tot}}/2} e^{-\Delta\omega_{12}} \frac{P_2}{P_{\text{tot}}} - \frac{P_1}{P_{\text{tot}}}. \quad (\text{S31})$$

Inserting $\frac{P_1}{P_{\text{tot}}} = 1 - \frac{P_2}{P_{\text{tot}}}$ and $\frac{P_2}{P_{\text{tot}}}$ from Eq. S30 into Eq. S31 and Taylor expanding for small $\Delta\omega_{12}$ gives

$$J_{12} + J_{21} \simeq e^{\omega_{\text{tot}}/2} \left[1 + \left(\frac{1}{2} - \frac{1}{1 + e^{-\omega_{\text{tot}}/2}} \right) (\Delta\omega_{12})^2 + \frac{k_{\text{esc}} \Delta\omega_{12}}{4(1 + e^{\omega_{\text{tot}}/2})} \right] - 1. \quad (\text{S32})$$

We approximate the accumulated flux for $k_{\text{esc}} \frac{P_2}{P_{\text{tot}}} t \ll 1$ as

$$\Phi_{\text{acc}} = [J_{12}(t=0) + J_{21}(t=0)] \int_0^t e^{-k_{\text{esc}} \frac{P_2}{P_{\text{tot}}} t'} dt' \quad (\text{S33a})$$

$$\simeq [J_{12}(t=0) + J_{21}(t=0)] \left(t - \frac{k_{\text{esc}} \frac{P_2}{P_{\text{tot}}} t^2}{2} \right), \quad (\text{S33b})$$

with the second line dropping the $t=0$ for the J_{ij} . Inserting Eqs. S30 and S32, and their derivatives, into $\partial\Phi_{\text{acc}}/\partial\Delta\omega_{12} = 0$ (using Eq. S33b for Φ_{acc}), and dropping all terms of higher order than k_{esc} and $\Delta\omega_{12}$, produces Eq. 17 (reproduced here for convenience),

$$\frac{\Delta\omega_{12}^*}{k_{\text{esc}}} \simeq -\frac{1}{4} \left(t - \frac{1}{e^{\frac{1}{2}\omega_{\text{tot}}} - 1} \right). \quad (\text{S34})$$

A similar derivation for RL rate constants leads to Eq. 18,

$$\frac{\Delta\omega_{12}^*}{k_{\text{esc}}} \simeq -\frac{1}{4} \left(t + \frac{1}{1 - e^{-\frac{1}{2}\omega_{\text{tot}}}} \right). \quad (\text{S35})$$

We find the same equations using Maple 2016, keeping all non-Taylor expanded expressions, and then Taylor expanding the final derivative $\partial\Phi_{\text{acc}}/\partial\Delta\omega_{12} = 0$ for small k_{esc} and $\Delta\omega_{12}$.

For both FL and RL, escape is reduced by a more negative $\Delta\omega_{12}$. Reducing escape grows in importance for longer times, hence the negative sign of the t -dependent term in both Eqs. (S34) and (S35). For $\Delta\omega_{12} = 0$, escape causes $P_2 < P_1$ at steady state, leading $[\partial(J_{12} + J_{21})/\partial\omega_{12}]_{\Delta\omega_{12}=0}$ to be positive for FL (increasing the forward rate constant from the state with larger steady-state probability) and negative for RL (increasing the reverse rate constant from the state with larger steady-state probability). Hence the t -independent term in $\Delta\omega_{12}^*$ is positive for FL (Eq. (S34)) and negative for RL (Eq. (S35)). With FL and for large ω_{tot} , the forward rate constants are very large, so escape influences P_1 and P_2 negligibly at $\Delta\omega_{12}^* = 0$, so the t -independent term of Eq. (S34) decreases in magnitude towards zero as ω_{tot} increases. With RL and for large ω_{tot} , the reverse rate constants are very small, so the influence

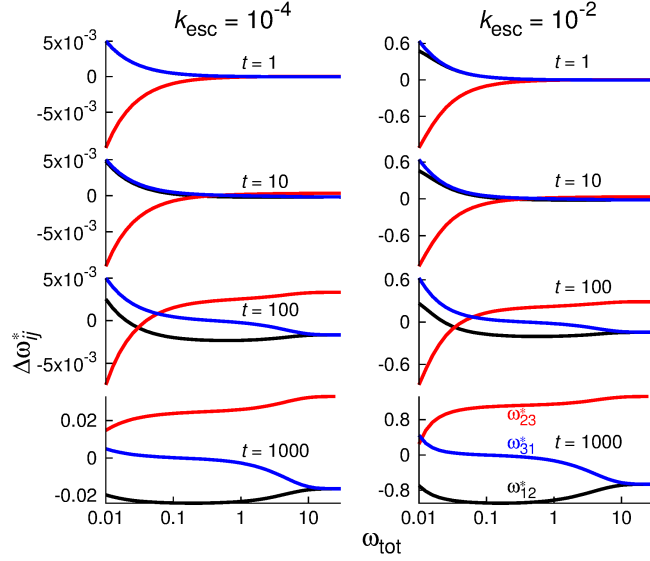


Figure S2: **Allocating free energy to maximize processivity of forward labile cycles.** Free energy allocation that maximizes accumulated flux up to time t (Eq. S40) through three-state forward labile cycle with state 2 vulnerable to escape. Bare rate constants $k_{12}^0 = k_{23}^0 = k_{31}^0 = 1$.

of escape on P_1 and P_2 becomes insensitive to ω_{tot} increases, so the t -independent term of Eq. (S35) decreases in magnitude to a constant value as ω_{tot} increases.

Three states

The three-state cycle with state 2 vulnerable to escape is governed by differential equations

$$\frac{dP_1}{dt} = -(k_{12}^+ + k_{31}^-)P_1 + k_{12}^-P_2 + k_{31}^+P_3 \quad (\text{S36a})$$

$$\frac{dP_2}{dt} = k_{12}^+P_1 - (k_{12}^- + k_{23}^+ + k_{\text{esc}})P_2 + k_{23}^-P_3 \quad (\text{S36b})$$

$$\frac{dP_3}{dt} = k_{31}^-P_1 + k_{23}^-P_2 - (k_{23}^- + k_{31}^+)P_3 . \quad (\text{S36c})$$

Substituting Eqs. S36a, S36b, S36c into Eq. S26 produces

$$\frac{d\left(\frac{P_1}{P_{\text{tot}}}\right)}{dt} = -(k_{12}^+ + k_{31}^-)\frac{P_1}{P_{\text{tot}}} + k_{12}^-\frac{P_2}{P_{\text{tot}}} + k_{31}^+\frac{P_3}{P_{\text{tot}}} + k_{\text{esc}}\frac{P_1}{P_{\text{tot}}}\frac{P_2}{P_{\text{tot}}} \quad (\text{S37a})$$

$$\frac{d\left(\frac{P_2}{P_{\text{tot}}}\right)}{dt} = k_{12}^+\frac{P_1}{P_{\text{tot}}} - (k_{12}^- + k_{23}^+ + k_{\text{esc}})\frac{P_2}{P_{\text{tot}}} + k_{23}^-\frac{P_3}{P_{\text{tot}}} + k_{\text{esc}}\left(\frac{P_2}{P_{\text{tot}}}\right)^2 \quad (\text{S37b})$$

$$\frac{d\left(\frac{P_3}{P_{\text{tot}}}\right)}{dt} = k_{31}^-\frac{P_1}{P_{\text{tot}}} + k_{23}^+\frac{P_2}{P_{\text{tot}}} - (k_{23}^- + k_{31}^+)\frac{P_3}{P_{\text{tot}}} + k_{\text{esc}}\frac{P_3}{P_{\text{tot}}}\frac{P_2}{P_{\text{tot}}} . \quad (\text{S37c})$$

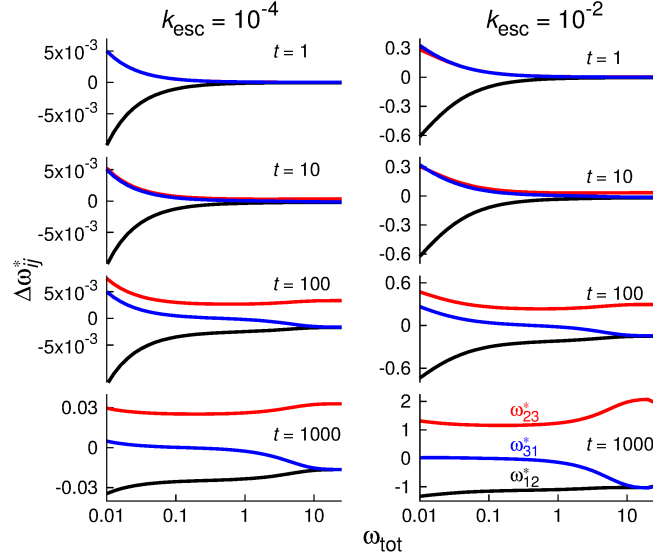


Figure S3: **Allocating free energy to maximize processivity of reverse labile cycles.** Free energy allocation that maximizes accumulated flux up to time t (Eq. S40) through three-state reverse labile cycle with state 2 vulnerable to escape. Bare rate constants $k_{12}^0 = k_{23}^0 = k_{31}^0 = 1$.

Setting $d(P_i/P_{\text{tot}})/dt = 0$ gives

$$\frac{P_1}{P_{\text{tot}}} = \frac{\left(k_{12}^+ k_{23}^- + k_{12}^+ k_{31}^+ + k_{23}^- k_{31}^- - k_{12}^- k_{\text{esc}} \frac{P_2}{P_{\text{tot}}}\right) \frac{P_2}{P_{\text{tot}}}}{k_{\text{esc}} \left(k_{\text{esc}} \frac{P_2}{P_{\text{tot}}} - k_{12}^+ - k_{23}^- - k_{31}^+ - k_{31}^- \right) \frac{P_2}{P_{\text{tot}}} + k_{12}^+ k_{23}^- + k_{12}^+ k_{31}^+ + k_{23}^- k_{31}^-}, \quad (\text{S38a})$$

$$\frac{P_3}{P_{\text{tot}}} = \frac{P_2}{k_{31}^+} \left[\left(k_{\text{esc}} \frac{P_2}{P_{\text{tot}}} - k_{12}^+ - k_{31}^- \right) \xi - k_{12}^- \right], \quad (\text{S38b})$$

$$\xi \equiv \frac{k_{\text{esc}} k_{12}^- \frac{P_2}{P_{\text{tot}}} - (k_{12}^- k_{23}^- + k_{12}^- k_{31}^+ + k_{23}^+ k_{31}^+)}{k_{\text{esc}}^2 \left(\frac{P_2}{P_{\text{tot}}}\right)^2 - k_{\text{esc}} (k_{12}^+ + k_{23}^- + k_{31}^+ + k_{31}^-) \frac{P_2}{P_{\text{tot}}} + k_{12}^+ k_{23}^- + k_{12}^+ k_{31}^+ + k_{23}^- k_{31}^-}. \quad (\text{S38c})$$

Substituting these equations into Eq. S37b produces a cubic equation for P_2/P_{tot} ,

$$\begin{aligned} & k_{\text{esc}}^2 \left(\frac{P_2}{P_{\text{tot}}}\right)^3 - k_{\text{esc}} (k_{12}^+ + k_{12}^- + k_{23}^+ + k_{23}^- + k_{31}^+ + k_{31}^- + k_{\text{esc}}) \left(\frac{P_2}{P_{\text{tot}}}\right)^2 \\ & + [k_{\text{esc}} (k_{12}^+ + k_{23}^- + k_{31}^+ + k_{31}^-) + k_{12}^+ k_{23}^- + k_{12}^+ k_{23}^+ + k_{12}^+ k_{31}^+ + k_{23}^- k_{31}^- + k_{12}^- k_{23}^- + k_{12}^- k_{31}^+ + k_{12}^- k_{31}^- \\ & + k_{23}^+ k_{31}^+ + k_{23}^+ k_{31}^-] \frac{P_2}{P_{\text{tot}}} - (k_{12}^+ k_{23}^- + k_{12}^+ k_{31}^+ + k_{23}^- k_{31}^-) = 0. \end{aligned} \quad (\text{S39})$$

Cubic equations generally have at least one real solution, so a real P_2/P_{tot} exists.

Solving the cubic for P_2/P_{tot} in Eq. S39 determines the steady-state P_i/P_{tot} and $P_{\text{tot}}(t)$. Because the flux decays with time as probability escapes, we additionally consider the rate of escape to evaluate molecular machine progress. Instead of flux alone, we combine flux and escape into the accumulated flux

$$\Phi_{\text{acc}} = \int_0^t [J_{12}(t') + J_{23}(t') + J_{31}(t')] dt', \quad (\text{S40})$$

which we maximize after a time t . Figs. S2 (FL cycles) and S3 (RL cycles) show ω_{ij} allocations which maximize Φ_{acc} . These three-state results are similar to the two-state results in the main text.

References

- (1) Clancy, B. E.; Behnke-Parks, W. M.; Andreasson, J. O. L.; Rosenfeld, S. S.; Block, S. M. Pathway for kinesin stepping. *Nat. Struct. Mol. Biol.* **2011**, *18*, 1020–1027.
- (2) Caruthers, J. M.; McKay, D. B. Helicase structure and mechanism. *Curr. Opin. Struct. Biol.* **2002**, *12*, 123–133.
- (3) Cardozo, T.; Pagano, M. The SCF ubiquitin ligase: insights into a molecular machine. *Nat. Rev. Mol. Cell Biol.* **2004**, *5*, 739–751.
- (4) Boyer, P. D. The ATP synthase — a splendid molecular machine. *Annu. Rev. Biochem.* **1997**, *66*, 717–749.
- (5) Fernie, A. R.; Carrari, F.; Sweetlove, L. J. Respiratory metabolism: glycolysis, the TCA cycle and mitochondrial electron transport. *Curr. Opin. Plant Biol.* **2004**, *7*, 254–261.
- (6) Vale, R. D.; Milligan, R. A. The way things move: looking under the hood of molecular motor proteins. *Science* **2000**, *288*, 88–95.
- (7) Bustamante, C.; Keller, D.; Oster, G. The physics of molecular motors. *Acc. Chem. Res.* **2001**, *34*, 412–420.
- (8) Astumian, R. D.; Bier, M. Fluctuation driven ratchets: molecular motors. *Phys. Rev. Lett.* **1994**, *72*, 1766–1769.
- (9) Isojima, H.; Iino, R.; Niitani, Y.; Noji, H.; Tomishige, M. Direct observation of intermediate states during the stepping motion of kinesin-1. *Nat. Chem. Biol.* **2016**, *12*, 290–297.
- (10) Fisher, M. E.; Kolomeisky, A. B. The force exerted by a molecular motor. *Proc. Natl. Acad. Sci. USA* **1999**, *96*, 6597–6602.
- (11) Schmiedl, T.; Seifert, U. Efficiency of molecular motors at maximum power. *Europhys. Lett.* **2008**, *83*, 30005.
- (12) Wagoner, J. A.; Dill, K. A. Molecular motors: power strokes outperform Brownian ratchets. *J. Phys. Chem. B* **2016**, *120*, 6327–6336.
- (13) Astumian, R. D. Irrelevance of the power stroke for the directionality, stopping force, and optimal efficiency of chemically driven molecular machines. *Biophys. J.* **2015**, *108*, 291–303.
- (14) Thomas, N.; Imafaku, Y.; Tawada, K. Molecular motors: thermodynamics and the random walk. *Proc. R. Soc. Lond. B* **2001**, *268*, 2113–2122.
- (15) Astumian, R. D.; Mukherjee, S.; Warshel, A. The physics and physical chemistry of molecular machines. *ChemPhysChem* **2016**, *17*, 1719–1741.
- (16) Xing, J.; Wang, H.; Oster, G. From continuum Fokker-Planck models to discrete kinetic models. *Biophys. J.* **2005**, *89*, 1551–1563.
- (17) Nguyen, V.; Wilson, C.; Hoemberger, M.; Stiller, J. B.; Agafonov, R. V.; Kutter, S.; English, J.; Theobald, D. L.; Kern, D. Evolutionary drivers of thermoadaptation in enzyme catalysis. *Science* **2017**, *355*, 289–294.

- (18) Milic, B.; Andreasson, J. O. L.; Hancock, W. O.; Block, S. M. Kinesin processivity is gated by phosphate release. *Proc. Natl. Acad. Sci. USA* **2014**, *111*, 14136–14140.
- (19) Kolomeisky, A. B.; Fisher, M. E. A simple kinetic model describes the processivity of myosin-V. *Biophys. J.* **2003**, *84*, 1642–1650.
- (20) Qian, H. Open-system nonequilibrium steady state: statistical thermodynamics, fluctuations, and chemical oscillations. *J. Phys. Chem. B* **2006**, *110*, 15063–15074.
- (21) Phillips, R.; Kondev, J.; Theriot, J.; Garcia, H. *Physical Biology of the Cell*, 2nd ed.; Garland Science, 2012.
- (22) Pietzonka, P.; Barato, A. C.; Seifert, U. Universal bound on the efficiency of molecular motors. *J. Stat. Mech: Theory Exp.* **2016**, 124004.
- (23) Rao, R.; Esposito, M. Nonequilibrium thermodynamics of chemical reaction networks: wisdom from stochastic thermodynamics. *Phys. Rev. X* **2016**, *6*, 041064.
- (24) Hill, T.; Eisenberg, E. Can free energy transduction be localized at some crucial part of the enzymatic cycle? *Q. Rev. Biophys.* **1981**, *14*, 463–511.
- (25) Hill, T. Some general principles in free energy transduction. *Proc. Natl. Acad. Sci. USA* **1983**, *80*, 2922–2925.
- (26) Brown, A. I.; Sivak, D. A. Allocating dissipation across a molecular machine cycle to maximize flux. *Proc. Natl. Acad. Sci. USA* **2017**, *114*, 11057–11062.
- (27) Hill, T. *Free Energy Transduction in Biology: Steady State Kinetic and Thermodynamic Formalism*; Academic Press, 1977.
- (28) Hodges, A. R.; Krementsova, E. B.; Trybus, K. M. Engineering the processive run length of myosin V. *J. Biol. Chem.* **2007**, *282*, 27192–27197.
- (29) Andreasson, J. O. L.; Milic, B.; Chen, G.-Y.; Gwydosh, N. R.; Hancock, W. O.; Block, S. M. Examining kinesin processivity within a general gating framework. *eLife* **2015**, *4*, e07403.
- (30) Muthukrishnan, G.; Zhang, Y.; Shastry, S.; Hancock, W. O. The processivity of kinesin-2 motors suggests diminished front-head gating. *Proc. Natl. Acad. Sci. USA* **2015**, *112*, E6606–E6613.
- (31) Nam, W.; Epureanu, B. I. Highly loaded behavior of kinesins increases the robustness of transport under high resisting loads. *PLoS Comput. Biol.* **2015**, *11*, e1003981.
- (32) Topraka, E.; Yildiz, A.; Hoffman, M. T.; Rosenfeld, S. S.; Selvin, P. R. Why kinesin is so processive. *Proc. Natl. Acad. Sci. USA* **2009**, *106*, 12717–12722.
- (33) Hinczewski, M.; Tehver, R.; Thirumalai, D. Design principles governing the motility of myosin V. *Proc. Natl. Acad. Sci. USA* **2013**, *110*, E4059–E4068.
- (34) Zimmermann, E.; Seifert, U. Efficiencies of a molecular motor: a generic hybrid model applied to the F₁-ATPase. *New J. Phys.* **2012**, *14*, 103023.
- (35) Fisher, M. E.; Kolomeisky, A. B. Simple mechanochemistry describes the dynamics of kinesin molecules. *Proc. Natl. Acad. Sci. USA* **2001**, *98*, 7748–7753.

- (36) Hwang, W.; Hyeon, C. Quantifying the heat dissipation from a molecular motor's transport properties in nonequilibrium steady states. *J. Phys. Chem. Lett.* **2017**, *8*, 250–256.
- (37) Liepelt, S.; Lipowsky, R. Kinesin's network of chemomechanical motor cycles. *Phys. Rev. Lett.* **2007**, *98*, 258102.
- (38) Lau, A. W. C.; Lacoste, D.; Mallick, K. Nonequilibrium fluctuations and mechanochemical couplings of a molecular motor. *Phys. Rev. Lett.* **2007**, *99*, 158102.
- (39) Singh, M. P.; Mallik, R.; Gross, S. P.; Yu, C. C. Modeling of single-molecule cytoplasmic dynein. *Proc. Natl. Acad. Sci. USA* **2005**, *102*, 12059–12064.
- (40) Visscher, K.; Schnitzer, M. J.; Block, S. M. Single kinesin molecules studied with a molecular force clamp. *Nature* **1999**, 184–189.
- (41) Carter, N. J.; Cross, R. A. Mechanics of the kinesin step. *Nature* **2005**, *435*, 308–312.
- (42) Wang, Q.; Diehl, M. R.; Jana, B.; Cheung, M. S.; Kolomeisky, A. B.; Onuchic, J. N. Molecular origin of the weak susceptibility of kinesin velocity to loads and its relation to the collective behavior of kinesins. *Proc. Natl. Acad. Sci. USA* **2017**,
- (43) Mukherjee, S.; Alhadeff, R.; Warshel, A. Simulating the dynamics of the mechanochemical cycle of myosin-V. *Proc. Natl. Acad. Sci. USA* **2017**, *114*, 2259–2264.
- (44) Thorn, K. S.; Ubersax, J. A.; Vale, R. D. Engineering the processive run length of the kinesin motor. *J. Cell Biol.* **2000**, *151*, 1093–1100.
- (45) Schnitzer, M. J.; Block, S. M. Kinesin hydrolyses one ATP per 8-nm step. *Nature* **1997**, *388*, 386–390.
- (46) Hill, T. L. Interrelations between random walks on diagrams (graphs) with and without cycles. *Proc. Natl. Acad. Sci. USA* **1988**, *85*, 2879–2883.